The behavior of runaway current in massive gas injection fast shutdown plasmas in J-TEXT

2016 Nucl. Fusion 56 112013

(http://iopscience.iop.org/0029-5515/56/11/112013)

IOP Publishing | International Atomic Energy Agency Nuclear Fusion

Nucl. Fusion **56** (2016) 112013 (10pp) doi:10.1088/0029-5515/56/11/112013

The behavior of runaway current in massive gas injection fast shutdown plasmas in J-TEXT

Z.Y. Chen[1], D.W. Huang[1], Y.H. Luo[1], Y. Tang[1], Y.B. Dong[2], L. Zeng[3], R.H. Tong[1], S.Y. Wang[1], Y.N. Wei[1], X.H. Wang[1], X. Jian[1], J.C. Li[1], X.Q. Zhang[1], B. Rao[1], W. Yan[1], T.K. Ma[1], Q.M. Hu[1], Z.J. Yang[1], L. Gao[1], Y.H. Ding[1], Z.J. Wang[1], M. Zhang[1], G. Zhuang[1], Y. Pan[1], Z.H. Jiang[1] and J-TEXT Team

[1] State Key Laboratory of Advanced Electromagnetic Engineering and Technology, School of Electrical and Electronic Engineering, Huazhong University of Science and Technology, Wuhan 430074, People's Republic of China

[2] Southwestern Institute of Physics, PO Box 432, Chengdu 610041, People's Republic of China

[3] Institute of Plasma Physics, Chinese Academy of Sciences, Hefei 230031, People's Republic of China

E-mail: zhhjiang@hust.edu.cn

Received 9 December 2015, revised 13 February 2016
Accepted for publication 15 February 2016
Published 22 July 2016

Abstract

Runaway currents following disruptions have an important effect on the first wall in current tokamaks and will be more severe in next generation tokamaks. The behavior of runaway currents in massive gas injection (MGI) induced disruptions have been investigated in the J-TEXT tokamak. The cold front induced by the gas jet penetrates helically along field lines, preferentially toward the high field side and stops at a location near the $q = 2$ surface before the disruption. When the cold front reaches the $q = 2$ surface it initiates magnetohydrodynamic activities and results in disruption. It is found that the MGI of He or Ne results in runaway free shutdown in a large range of gas injections. Mixture injection of He and Ar (90% He and 10%Ar) consistently results in runaway free shutdown. A moderate amount of Ar injection could produce significant runaway current. The maximum runaway energy in the runaway plateau is estimated using a simplified model which neglects the drag forces and other energy loss mechanisms. The maximum runaway energy increases with decreasing runaway current. Imaging of the runaway beam using a soft x-ray array during the runaway current plateau indicates that the runaway beam is located in the center of the plasma. Resonant magnetic perturbation (RMP) is applied to reduce the runaway current successfully during the disruption phase in a small scale tokamak, J-TEXT. When the runaway current builds up, the application of RMP cannot decouple the runaway beam due to the lower sensitivity of the energetic runaway electrons to the magnetic perturbation.

Keywords: runaway electron, disruption, massive gas injection

(Some figures may appear in colour only in the online journal)

1. Introduction

A plasma disruption in a tokamak is the sudden loss of magnetic confinement which results in a rapid, complete loss of the plasma's thermal and magnetic energy [1, 2]. The disruption is initiated by a global instability that causes a rapid thermal quench (TQ) of the plasma kinetic energy. The resulting resistive plasma causes the confining poloidal magnetic field to decay during the current quench (CQ). The disruption may cause damage by the following means: (1) plasma-conducted

thermal loading of the divertor surface during the TQ, (2) $J \times B$ forces from vessel poloidal halo currents during the CQ and (3) the conversion of toroidal plasma current into energetic runaway electrons (REs) that are eventually stopped by the first wall [3–5]. The magnitude of the damaging effects increases with the plasma thermal energy W_{th} and magnetic energy W_{mag} [4, 5]. The avoidance and mitigation of disruptions are critical issues for advancing the concept of the tokamak as a viable fusion energy source. Prevention and mitigation of the damage due to disruptions are essential for reliable operation of International Thermonuclear Experimental Reactor (ITER) due to the high thermal and poloidal magnetic energy content of the plasma [6]. Both the heat loads and the electromagnetic force have been mitigated with a moderate amount of massive gas injection (MGI) of impurities [4]. It is generally thought that the heat load and halo current reduction capabilities of MGI shutdown will scale well to ITER [3]. Although the generation of REs is typically found to be very small during intensive MGI shutdowns, the number of electrons (free + bound) injected by the MGI prior to the CQ is estimated to be insufficient to achieve RE suppression by collision damping in present-day machines.

The potentially damaging consequences of the large runaway currents generated by disruptions are still a serious issue for next generation devices. There are, generally, three mechanisms for RE generation: primary generation (Dreicer generation), secondary generation (avalanche generation) and hot tail generation [7–9]. In a disruption, the Dreicer and the hot tail processes create a runaway seed population which is amplified by the secondary avalanche mechanism. The hot tail process can contribute significantly to runaway generation in fast shutdown experiments [10–13]. The high electric fields induced during the CQ phase of a tokamak disruption can generate a large number of REs. A severe consequence of a disruption on ITER could be the generation of a 10 MA RE beam with energies of several tens of MeV that could damage the vacuum vessel and the structures of the machine if it were to hit the wall unmitigated [8]. Many experiments have been pursued toward understanding the physics of RE production, transport and amplification during disruptions [3, 14–22].

The behavior of runaway currents in MGI fast shutdown experiments have recently been investigated in the J-TEXT tokamak. This paper is organized as follows. An introduction to the J-TEXT tokamak is presented in section 2. The regime of runaway generation and the behavior of runaway beams in fast shutdown experiments are presented in section 3. The effect of resonant magnetic perturbation (RMP) on runaway suppression during disruption and during the runaway current plateau is presented in section 4. Finally, a summary is presented in section 5.

2. Experimental set-up

Joint Texas Experimental Tokamak (J-TEXT) is a conventional tokamak with an iron core [23]. It has a major radius of $R = 105$ cm. The minor radius can be modified in the range of 25–29 cm by a movable titanium–carbide coated graphite limiter. The maximum toroidal magnetic field is $B_T = 2.3$ T. The maximum plasma current is $I_p = 220$ kA with a 600 ms pulse length. The line averaged electron density is in the range of $n_e = (1\text{–}6) \times 10^{19}$ m^{-3}.

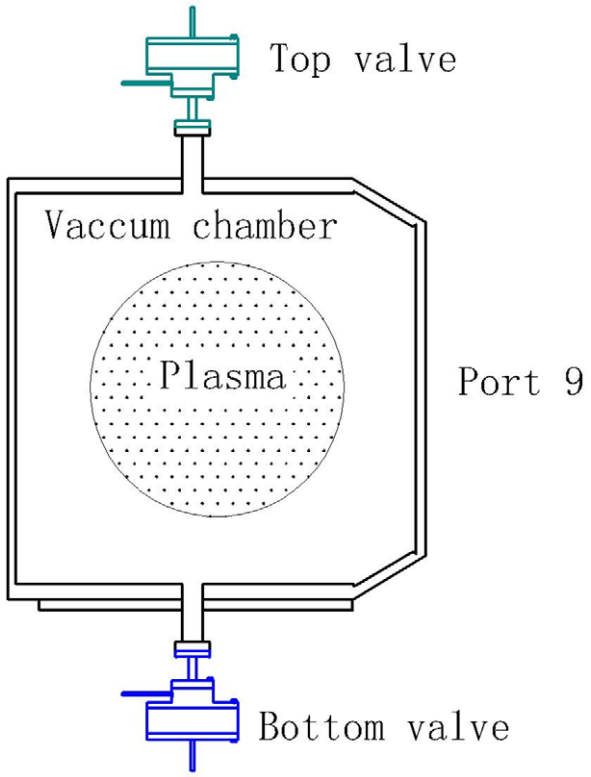

Figure 1. Schematic view of the MGI valves on J-TEXT. A 30 ml MGI valve is installed at the bottom of port 9. Another 60 ml MGI valve is installed at the top of port 9.

A multichannel far-infrared (FIR) interferometer with seven channels crossing the J-TEXT cross-section vertically is employed to measure the electron density. There are two poloidal arrays of 2D Mirnov coils and one toroidal array mounted inside the vessel for detection of magnetohydrodynamic (MHD) activities. Three absolute extreme ultraviolet (AXUV) arrays are used to measure the total radiated power and the radiation profile. The hard x-ray radiation (HXR) in the energy range of 0.5–5 MeV, resulting from the thick target bremsstrahlung when REs are lost from the plasma and impinge on the vessel walls, is measured using two NaI detectors. One NaI detector is arranged in the electron approach direction. The other one is arranged in the radial direction. In order to prevent the saturation of the detector, a 1 cm thick lead brick is placed in front of the collimator. Thus the low energy HXR is cutoff in the measurement. A vertical soft x-ray pinhole camera located at the top of the vessel is used to measure the runaway beam generated by the disruption. This is used to measure the profile of the soft x-ray emission and the sawtooth activities. There are two sets of RMP systems for studying the effect on the magnetic topology as well as the transport [23]. The static RMP coils are located outside the vessel. The dynamic RMP coils are located inside the vessel and can be operated in both the DC and AC modes.

Two MGI valves have been developed for the study of the plasma fast shutdown experiments on the J-TEXT tokamak. A schematic view of the MGI valves is shown in figure 1.

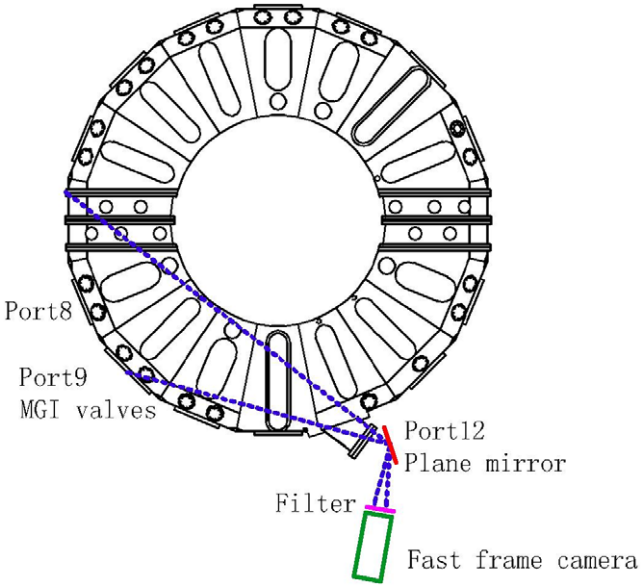

Figure 2. Schematic view of the fast frame camera diagnostics on J-TEXT.

A 30 ml MGI valve is installed at the bottom port of port 9. It can be operated in the range of 5–30 bar. Another 60 ml MGI valve is installed at the top port of port 9. It can be operated in the range of 5–40 bar. It is based on the eddy-current repulsion mechanism. The piston of the MGI valve is made from a non-ferromagnetic material so that it can be installed as close as to the vacuum vessel as possible. The valves are about 0.5 m away from the plasma boundary. An important feature of the MGI valve is that the coil is installed separately with the mushroom cap of the piston and connected with the atmosphere [24]. Thus the temperature of the coils can be kept at a low value. The pulse current is produced by a discharge circuit which is triggered by a central control system. A high speed camera is used to calibrate the moving distance of the piston. It shows that the reaction time of the MGI valve is about 0.3 ms. The MGI valve can keep opening in the order of 10 ms. The maximum density of the injected purities is more than 100 times the plasma inventory.

A fast frame camera (Phantom V710) is installed at the middle plane of port 12 which has a tangential view to port 9 where the MGI valves are located. A schematic view of the fast frame camera diagnostics is shown in figure 2. The fast frame camera can be operated with 22 000 fps (frames per second) with a 640 × 480 pixel resolution. The penetration process of the gas jet from the plasma boundary to the core can be studied by covering a special filter on the camera lens. For argon MGI fast shutdown experiments, a filter with a center wave length of 442.6 nm is used. It has a peak transmittance of about 65% with a 2 nm FWHM.

3. Behavior of REs in fast shutdown experiments

For disruption mitigation using MGI, several kinds of impurities have been used in different machines. He, Ne, Ar and gas mixtures are good candidates for disruption mitigation for different purposes. The massive injection of low Z impurities has the advantages of slow CQ and an increase of the electron density. It is favorable for the suppression of REs. But its ability to radiate energy is very limited. The massive injection of high Z impurities has the advantage of high efficiency on energy radiation and fast CQ, which is favorable for the reduction of halo current. However, it is prone to induce REs due to the fast CQ rate. The injection of mixtures of gases has the advantages of both energy radiation and runaway suppression.

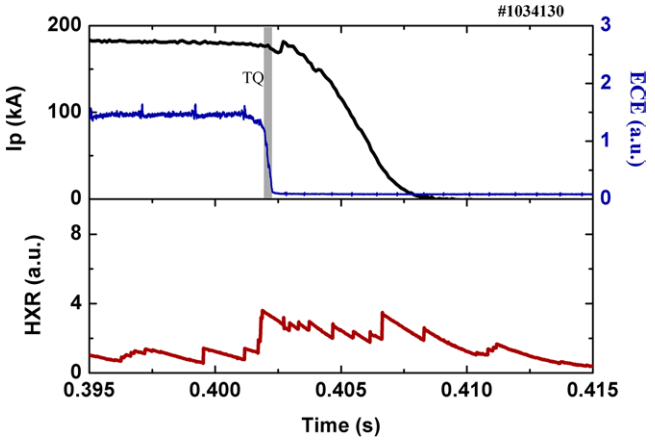

Figure 3. Fast shutdown experiments using pure He with about 4×10^{20} He injection. The CQ rate is about 46 MA s^{-1}.

He, Ne, Ar and gas mixture injections were performed in the fast shutdown experiment on J-TEXT. In this experiment, the target plasmas have a toroidal magnetic field $B_T = 2.3$ T, the plasma current is $I_p = 180$ kA and the line averaged electron density is about $n_e = (1.0–1.2) \times 10^{19}$ m^{-3}. The fast valve located at the bottom of port 9 was used in this experiment. The MGI was fired at 0.4 s in all plasma targets.

The typical waveforms of the fast shutdown with about 4×10^{20} He atom injection are shown in figure 3. The plasma was disrupted in 2.7 ms. The fast drops of the center electron cyclotron emission (ECE) signal and the plasma current indicate the TQ phase and CQ phase, respectively. The TQ duration is about 0.24 ms. The CQ rate is about 46 MA s^{-1}. The absence of ECE emission, the fast decay of the current tail and the negligible HXR flux at the end of the CQ phase indicate that the He injection results in runaway free shutdown. The dependence of the disruption delay time and the CQ rate on the amount of gas injection has been studied, as shown in figure 4. Here the disruption delay time is defined as the time delay between the current spike and the firing of MGI. The injected atoms increased with increasing high voltage (HV) applied on the MGI valve. It was found that the CQ rate increased from 10 MA s^{-1} to about 50 MA s^{-1} with increasing MGI HV since the injected He gas increased. The disruption delay time decreased from 4.8 ms to about 2.8 ms with increasing gas injection. The plasma fast shutdowns were always runaway free in the range of (0.3–4) × 10^{20} He injection.

For the fast shutdown experiment with pure Ne MGI injection, the plasmas were runaway free in the range of (0.3–4) × 10^{20} Ne injection. The typical waveforms of the fast shutdown with about 4×10^{20} Ne atom injection are shown in figure 5. The plasma was disrupted in 2.9 ms. The CQ rate was about 56 MA s^{-1}. The absent of ECE emission, the fast

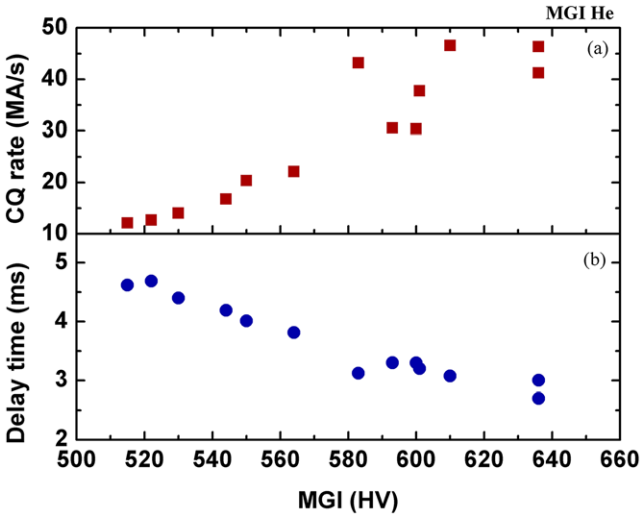

Figure 4. Dependence of the CQ rate and the disruption delay time on the amount of He injection. (*a*) is the CQ rate and (*b*) is the disruption delay time with respect to the time of firing MGI.

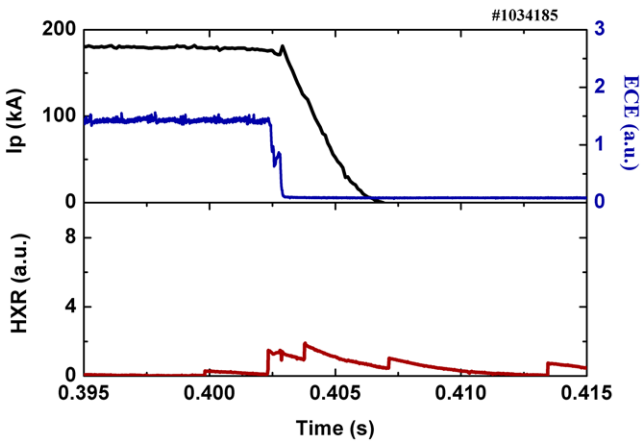

Figure 5. Fast shutdown experiments using pure Ne with about 4×10^{20} Ne injection. The CQ rate is about 56 MA s^{-1}.

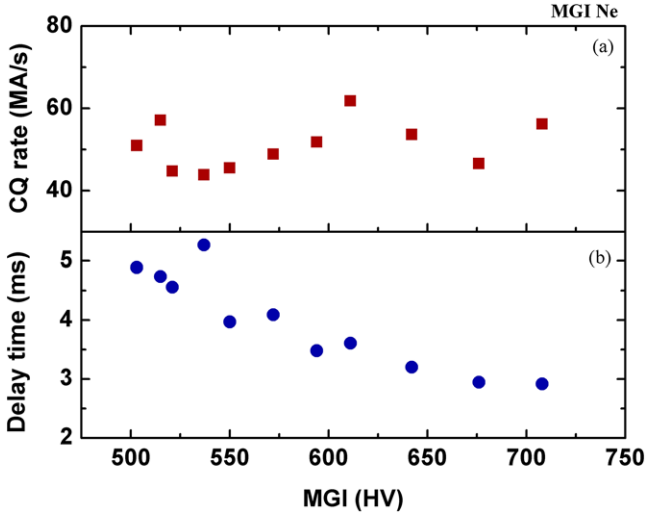

Figure 6. Dependence of the CQ rate and the disruption delay time on the amount of Ne injection. (*a*) is the CQ rate and (*b*) is the disruption delay time with respect to the time of firing MGI.

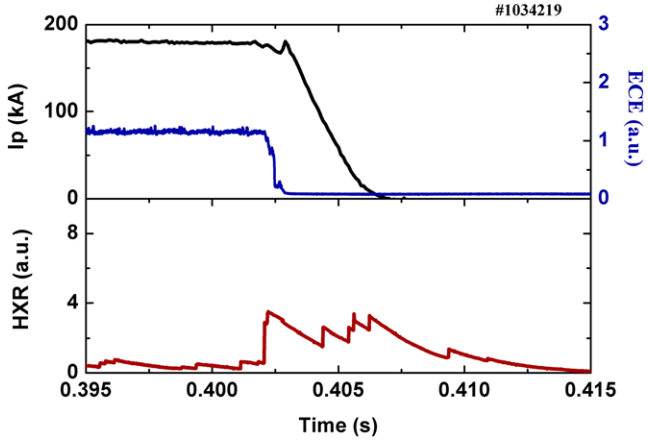

Figure 7. Typical waveforms of fast shutdown using mixture of He and Ar (9:1). The CQ rate is about 68 MA s^{-1}.

decay of current tail and the negligible HXR flux at the end of the CQ phase indicate that the Ne injection also results in runaway free shutdown. It was found that the CQ rate in Ne fast shutdown is not sensitive to the amount of gas injection in the investigated range, as shown in figure 6. The CQ rate was in the range of 40–60 MA s^{-1}. The disruption delay time decreased from 5 ms to about 3 ms with increasing gas injection.

In disruption mitigation, the heat load as well as REs should be mitigated at the same time. The mixture of low *Z* impurities with high *Z* impurities has been proved to have benefits in this issue. The low *Z* impurities contribute to the suppression of REs while the high *Z* impurities contribute to the radiation of plasma energy. A fast shutdown using a mixture of He and Ar was performed on J-TEXT. The mixture gas consisted of 90% He and 10% Ar. There were runaway free disruptions in the range of (0.3–4) $\times 10^{20}$ He and Ar injection. The typical waveforms of fast shutdowns using a mixture of He & Ar (9:1) are shown in figure 7. The absent of ECE emission, the fast decay of current tail, and the negligible HXR flux at the end of CQ phase indicate that the injection of a gas mixture also leads to runaway free shutdown. The CQ rate with gas mixture injection is much higher than that with pure He injection even with moderate gas injection, as shown in figure 8. The disruption delay time decreased from 4.5 ms to about 3 ms with increasing gas injection.

For pure argon MGI injection, the runaway current plateau was induced with moderate argon injection. The regime of runaway generation in an argon fast shutdown experiment is shown in figure 9. The runaway current can be induced when the number of injected argon atoms is larger than 1×10^{20}. The induced runaway current decreased with increasing argon atom injection. When the number of injected argon atoms was above 1×10^{21} the runaway current was suppressed. The plasma inventory before the firing of MGI is estimated to be about 1.5×10^{19}. The regime of runaway generation by argon injection is about 7–70 times the plasma inventory. The conversion ratio of predisruption plasma current into runaway current in most argon induced disruptions is in the range of 30%–60%.

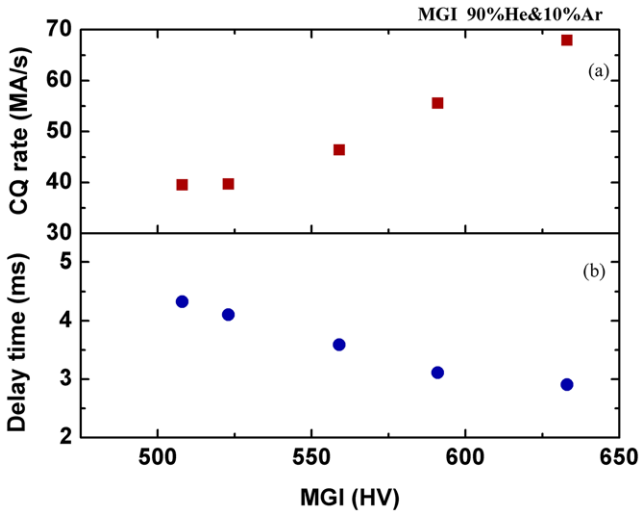

Figure 8. Dependence of the CQ rate and the disruption delay time on the amount of He and Ar (9:1) mixture injection. (*a*) is the CQ rate and (*b*) is the disruption delay time with respect to the time of MGI firing.

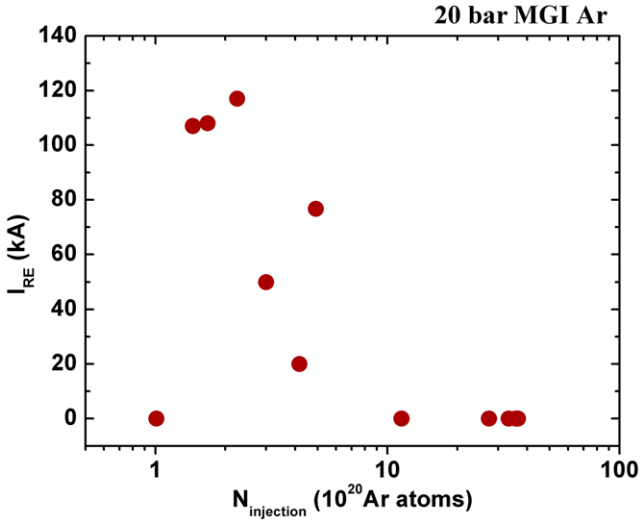

Figure 9. Dependence of the runaway current amplitude on the number of injected argon atoms.

The generation of runaway current in disruption depends on the plasma parameters. Several previous experimental observations have shown that there is a magnetic field threshold of $B_T = 2.0$ T for RE generation in tokamak disruptions [1, 3, 9, 25, 26]. Some recent results from Tokamak Experiment for Technology Oriented Research (TEXTOR), Korea Superconductivity Tokamak Advanced Research (KSTAR) and Joint European Torus (JET) indicate that the threshold is not robust [27–29]. The runaway generation can be formed with a much lower toroidal magnetic field than 2 T. The effect of the toroidal magnetic field B_T and the edge safety factor q_a on the generation of REs was investigated in J-TEXT as shown in figure 10. In order to prevent plasma density affecting runaway generation, the plasma density was kept at about 1×10^{19} m^{-3} which is favorable for the generation of runaways. It was found that the runaways can be generated with a much lower magnetic field $B_T = 1.6$ T.

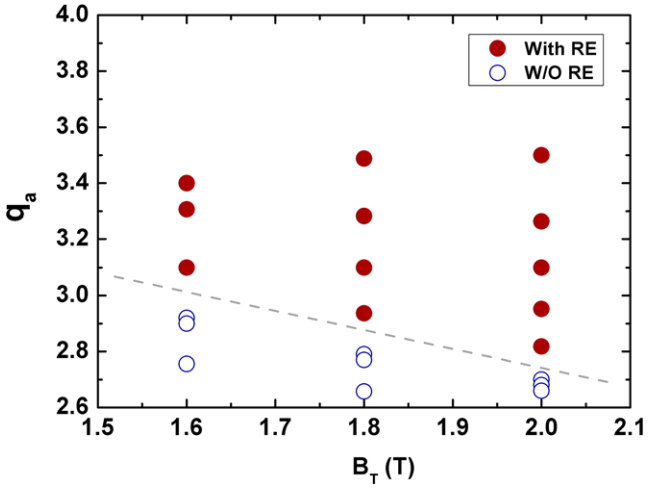

Figure 10. The regime of runaway generation for q_a versus B_T.

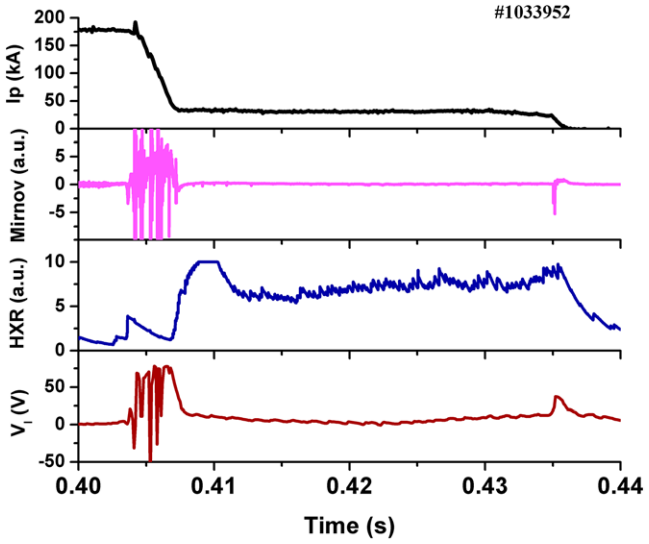

Figure 11. Disruption with a stable runaway current plateau using argon injection.

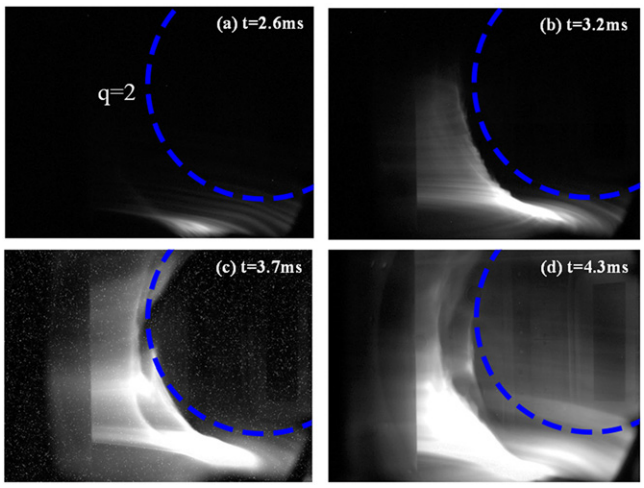

Figure 12. Observation of the penetration of the gas jet following disruption using a fast frame camera with a filter in front of the camera lens. The times on the images refer to the time of firing of the fast valve. The location of the $q = 2$ surface estimated using EFIT is plotted in the images.

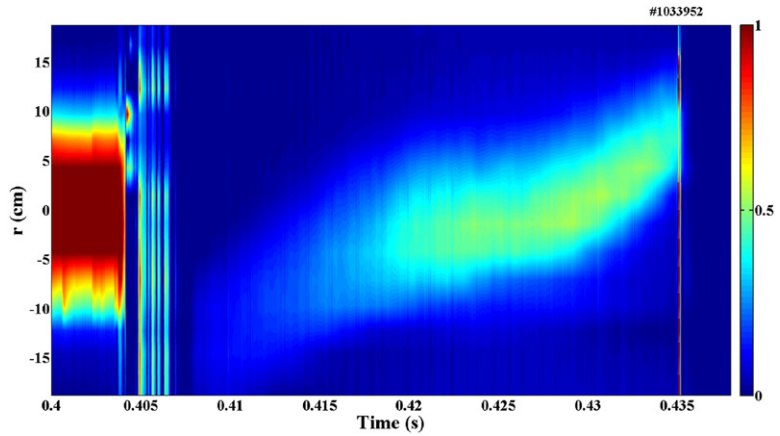

Figure 13. Soft x-ray image of the runaway beam during the runaway current plateau for discharge No. 1033952.

The effect of magnetic fluctuation on the runaway generation threshold cannot explain the result on J-TEXT [18]. The key parameter affecting runaway generation is the edge safety factor q_a instead of B_T in J-TEXT. The threshold of q_a decreases with increasing B_T. The threshold of q_a at $B_T = 1.6$ T is about 3.1. The q_a threshold decreased to about 2.7 at $B_T = 2$ T. With a lower edge safety factor, the plasma becomes more unstable which is prone to result in runaway free disruptions.

In the following argon induced disruption experiment, the target plasmas have a toroidal magnetic field of $B_T = 2.3$ T, the plasma current is $I_p = 180$ kA and the line averaged electron density is about $n_e = (1.0–1.2) \times 10^{19}$ m^{-3}. The fast valve was fired at 0.4 s.

A typical argon injection induced disruption with a runaway current plateau is shown in figure 11. The plasma disrupted in 4 ms. In this disruption, an about 30 kA runaway current plateau was formed by argon injection. The runaway current plateau persisted for about 28 ms before it was lost to the first wall. There was a large flux of HXR when the runaway current built up. The interaction of the argon gas jet with plasma can be observed directly using a fast frame camera [30]. In this argon injection experiment a filter (442.6 nm) was installed on the lens of the fast frame camera. Figure 12 shows a series of images of the penetration of the gas jet before the disruption. A superimposition of the equilibrium $q = 2$ surface from an equilibrium fitting (EFIT) reconstruction on the fast camera images has been used to study the penetration process of the gas jet. There were strong emissions at the plasma bottom when the gas jet from the bottom valve reached the plasma boundary. When the gas jet went into the plasma interior, a cold front was induced. The cold front penetrated helically along field lines preferentially toward to the high field side which is consistent with the simulation by NIMROD (non-ideal MHD with rotation, open discussion) [31]. The $q = 2$ surface in discharge No. 1033952 is estimated to be about 0.68 a. When the cold front penetrates into 0.7 a, strong MHD activities, as shown in figure 11, were induced which resulted in the loss of confinement and a major disruption.

The HXR diagnostics were used to extensively measure the lost REs. The measurement of the confined runaway beam during the runaway current plateau could provide significant information on runaway generation and confinement. The soft x-ray emissions during the runaway current plateau offer the possibility

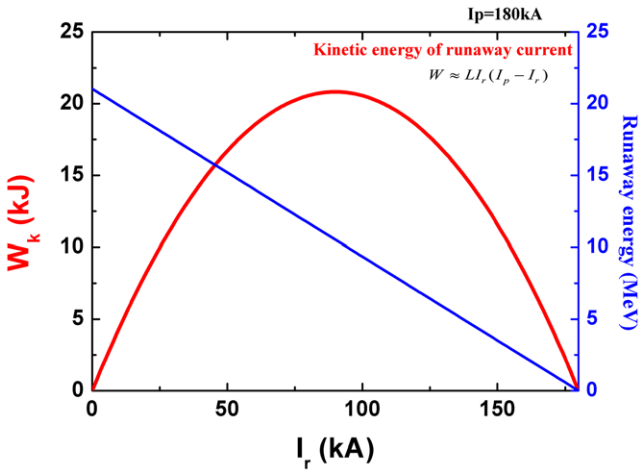

Figure 14. Dependence of the total kinetic energy of the runaway beam and the energy of a single RE versus the amplitude of the runaway current.

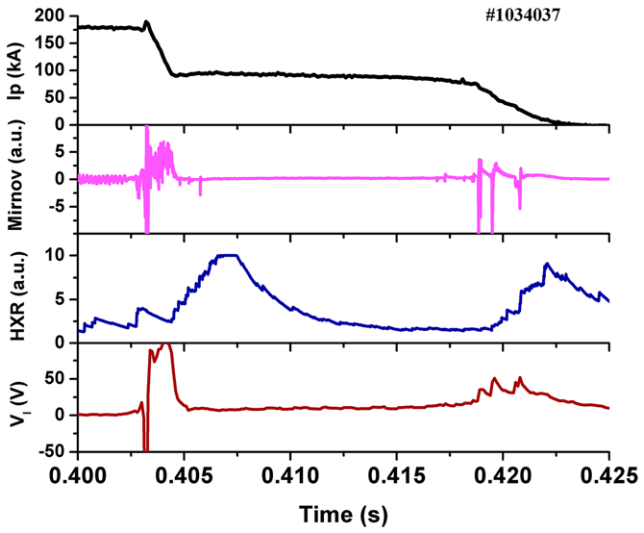

Figure 15. Disruption with a significant runaway current plateau using argon injection.

of investigating runaway beam generation and the beam size as a function of time [13, 32]. The RE beams produced weak x-ray images by producing K shell vacancies in impurities in the

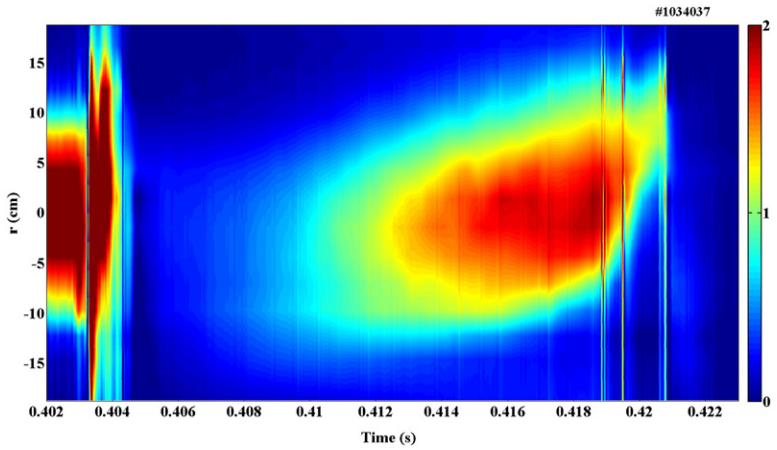

Figure 16. Soft x-ray image of the runaway beam during the runaway current plateau for discharge No. 1034037.

disrupted plasma that allowed us to determine the beam structure and the evolution of the beam using the soft x-ray (SXR) emissions. An image of the runaway beam using soft x-ray radiation for discharge No. 1033952 is shown in figure 13. According to the soft x-ray imaging, the plasma was disrupted at 0.404 s. The soft x-ray emissions increased slowly at the beginning of the runaway current plateau. The runaway beam is visible from 0.418 s in the soft x-ray image. For a 30 kA runaway plateau, the full width at half maximum (FWHM) of the SXR profile is about 12 cm. The runaway beam drifted to the low field side slowly from 0.428 s. The termination of the runaway current at 0.435 s can be directly observed in the soft x-ray image.

The fraction of predisruption plasma current converted into runaway current has an important effect on the runaway energy, which could affect the RE dissipation process. The maximum energy of REs built up during the current decay phase can be estimated by assuming the REs are generated at the beginning of the disruption and by neglecting the radiation losses, the collision damping and the change of inductance [33],

$$\delta W = ec\int E_{//}\mathrm{d}t \approx -\frac{ec}{2\pi R}\int L\frac{\mathrm{d}I_\mathrm{p}}{\mathrm{d}t}d_t \approx \frac{ecL}{2\pi R}(I_\mathrm{p}-I_\mathrm{r}).$$

Here L is the inductance, $L=\mu_0 R$ and I_r is the runaway current. This indicates that the energy of the REs decreases with increasing runaway current as shown in figure 14. The maximum runaway energy will reach its maximum value when the runaway current is close to zero. The maximum energy of REs in the 180 kA disruption plasma is about 21 MeV when the runaway current is in the order of a few kA.

The number of REs is about $N_\mathrm{r}\approx\frac{2\pi RI_\mathrm{r}}{ec}$. The total kinetic energy of the runaway beam is about $W\approx N_\mathrm{r}\delta W$, thus

$$W = N_\mathrm{r}\cdot\delta W = \frac{2\pi RI_\mathrm{r}}{ec}\cdot\frac{ecL}{2\pi R}(I_\mathrm{p}-I_\mathrm{r}) = LI_\mathrm{r}(I_\mathrm{p}-I_\mathrm{r}).$$

The total kinetic energy of the runaway beam increases with increasing runaway current. The runaway beam will reach its maximum kinetic energy when the runaway current is 50% of the predisruption plasma current. Then the kinetic energy of the runaway beam decreases with increasing runaway current when the runaway current is above 50% of the predisruption plasma current. The kinetic energy of the runaway beam for 30 kA runaway current is about 11.5 kJ. The maximum runaway energy is about 17.5 MeV for a 30 kA runaway current.

A typical fast shutdown using argon injection with significant runaway current is shown in figure 15. An about 90 kA runaway current was produced by argon injection. The runaway current persisted about 15 ms before being lost to the first wall. The fraction of predisruption plasma current converted to runaway current was about 50% in this shot. According to the results in figure 10, the kinetic energy of the runaway beam is estimated to reach the maximum $W_\mathrm{k}\sim 20.8$ kJ. The achievable maximum runaway energy is inversely proportional to the amplitude of the runaway current. The maximum runaway energy is about 10.5 MeV for a 90 kA runaway current.

A soft x-ray image of the runaway beam for discharge No. 1034037 is shown in figure 16. The soft x-rays become obvious at 0.41 s. The intensity of the soft x-ray image is much stronger compared to that with a 30 kA runaway current due to the larger number REs. For a 90 kA runaway plateau, the FWHM of the SXR profile is about 20 cm. The SXR profile of the 90 kA runaway plateau is much wider than that with a 30 kA runaway current. The termination of the runaway current from 0.419 s to 0.421 s with three MHD events can be directly observed using soft x-ray imaging.

The HXR flux during the runaway current plateau phase is lower compared to that with a 30 kA runaway current plateau. The increase of HXR flux from 405 ms to 408 ms at the early phase of runaway plateau formation is related to the prompt loss of runaways. At higher runaway current plateaus, the HXR flux is usually lower during the stable runaway current plateau phase. The HXR flux at different amplitudes of runaway plateau was analyzed as shown in figure 17. It was found that the HXR flux during the stable runaway current plateau phase decreases with an increasing runaway fraction. The final increase of HXR during the loss of runaway plateau is possibly related to the conversion of the magnetic energy of the runaway current into runaway kinetic energy [34].

4. Effect of RMP on runaway current

The suppression of runaway generation during disruption is essential for the next generation ITER device. RMP

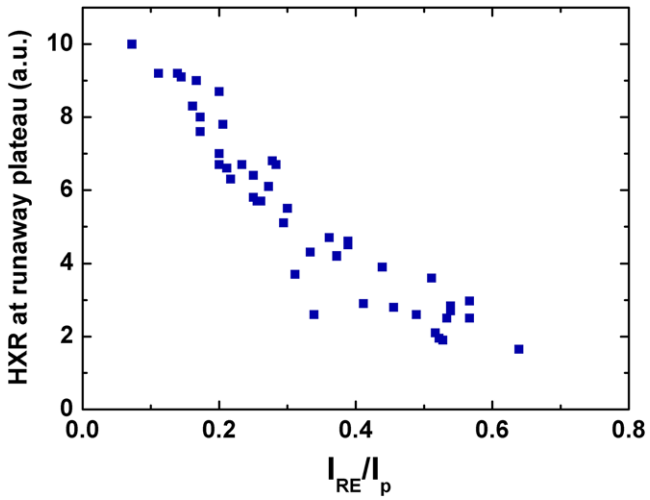

Figure 17. Dependence of the HXR flux on the amplitude of the runaway plateau during the stable runaway plateau phase.

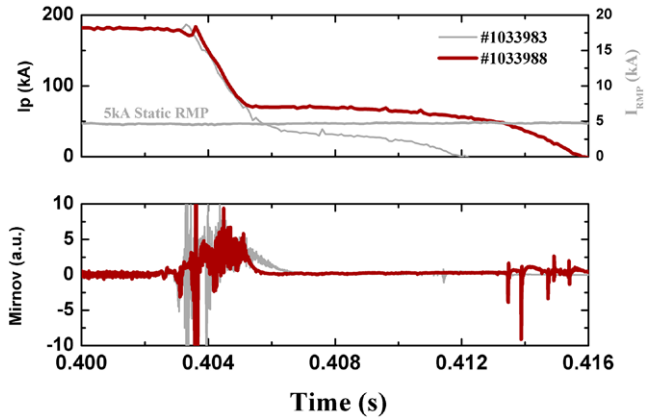

Figure 18. Waveforms of an argon induced runaway current plateau with/without the application of static RMP. The 5 kA static RMP with an $m/n = 2/1$ mode was powered from 0.38–0.43 s for shot No. 1033983. The static RMP coils can produce a 0.63 Gs kA^{-1} 2/1 mode. The application of static RMP during disruption reduced the runaway current.

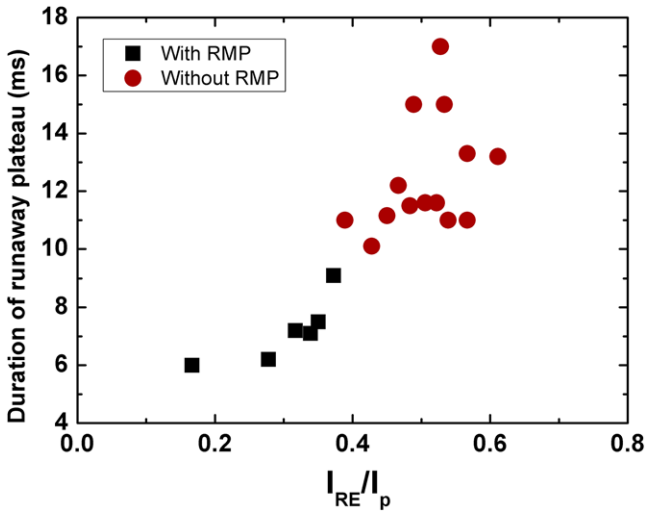

Figure 19. Duration of the runaway plateau versus the fraction of runaway current with or without the application of 5 kA static RMP ($\delta B/B_T = 1.3 \times 10^{-4}$). The plasma parameter is fixed at $B_T = 2.3$ T, $I_p = 180$ kA. The same MGI HV is applied for all targets. Both the amplitude and the duration of the runaway plateau decreased with the application of RMP.

is a powerful tool for the mitigation of ELMs. It has been proven that magnetic perturbation is a potential tool for the suppression of REs in JT-60U and TEXTOR [35–38]. The experimental results for TEXTOR have indicated that argon injection induced runaway current can be suppressed using RMP with sufficient strength [38]. However, RMP has not been successful in suppressing runaway generation during disruptions for the large device JET [39]. This is possibly due to the large distance from the RMP coils to the plasma and the large plasma size. Several simulations have been performed to investigate the mechanism of runaway suppression using RMP and the possibility of runaway suppression using RMP for next generation devices such as ITER [40–43]. The effects of RMP on runaway suppression were studied in J-TEXT to gain further understanding of the suppression effect in small scale device.

The enhancement of the runaway loss rate by the application of RMP with an $m/n = 2/1$ mode during the flat top phase has been demonstrated in J-TEXT [32]. It is found the runaway loss rate can be significantly enhanced when mode penetration occurs. The effect of RMP with an $m/n = 2/1$ mode on runaway generation during disruptions was investigated, and the application is shown in figure 18. The target plasma has a toroidal magnetic field of $B_T = 2.3$ T, the plasma current is $I_p = 180$ kA and the line averaged electron density is about $n_e = 1.0 \times 10^{19}$ m^{-3}. The fast valve is fired at 0.4 s with moderate argon injection to produce a stable runaway current plateau. In reference discharge No. 1033988, without the application of RMP, the runaway current plateau was about 70 kA. The runaway current persisted about 12 ms before being lost to the first wall. With the same plasma parameters and an equal amount of argon injection in discharge No. 1033983, a 5 kA static RMP was applied from 0.38 s to 0.43 s. The static RMP coils are located outside the vessel and can produce a 0.63 Gs kA^{-1} 2/1 mode. There was about 3 Gs $m/n = 2/1$ mode perturbation for this shot. This corresponds to $\delta B/B_T = 1.3 \times 10^{-4}$ magnetic perturbation. In order to prevent the generation of REs from the RMP, the outside RMP coils were powered from 0.38 s since RMP current need about 10 ms to ramp up. The runaway current was partially suppressed by the application of a $\delta B/B_T = 1.3 \times 10^{-4}$ magnetic perturbation during the disruption compared to reference discharge No.1033988 without the application of RMP. The amplitude of the runaway current plateau decreased from 70 kA to about 30 kA. The length of the runaway current plateau decreased from 12 ms to about 8 ms. The runaway plateau has a large decay rate in the RMP applied target as shown in figure 18. In this experiment there was no mode locking or mode penetration due to the limited strength of the applied RMP.

As to the amplitude and duration of the runaway plateau varied from shot to shot, even with same plasma parameters and argon injection, a statistical analysis of the effect of RMP on runaway suppression was performed, as shown in figure 19. Both the amplitude and the duration of the runaway

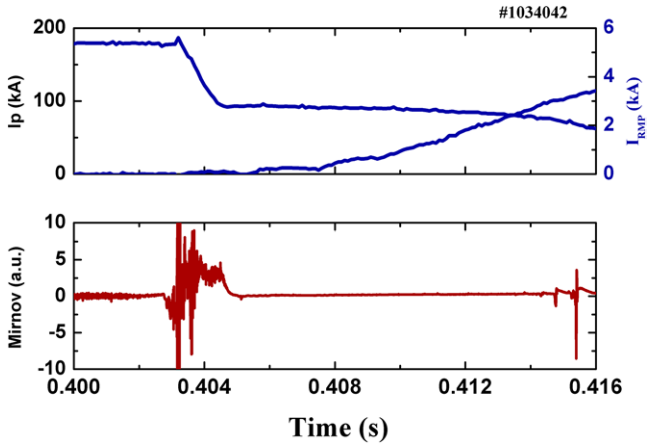

Figure 20. Typical waveforms of an argon induced runaway current plateau with the application of dynamic RMP during the runaway current plateau phase. The internal dynamic RMP coils can produce a 2.6 Gs kA^{-1} 2/1 mode. This corresponds to a $\delta B/B_T = 3.4 \times 10^{-4}$ magnetic perturbation with a 3 kA dynamic RMP.

current plateau decreased with the application of RMP. This indicates that the application of RMP reduces runaway production by enhancing runaway loss rate during the disruption in J-TEXT. RMP may not work for runaway suppression in large devices as the experiment in JET suggests that RMP is not effective for runaway suppression during disruptions on large machine [39]. The simulation of runaway suppression by RMP for ITER also predicted that RMP may not effective to achieve runaway suppression [41]. The success of runaway suppression using RMP in J-TEXT is possible due to its small size and the short distance between the RMP coils and the plasma.

Due to the large avalanche factor of next generation devices, the suppression of runaway generation during disruption will be a great challenge. The alternative is to allow runaway generation and hold the runaway current away from the first wall. Thus the dissipation of the runaway beam is preferred. The effect of RMP with an $m/n = 2/1$ mode on the confinement of runaway current was investigated in J-TEXT. A target plasma with a 90 kA runaway current plateau was initiated by argon injection at 0.4 s as shown in figure 20. The runaway current plateau formed at 0.405 s. In order to generate strong magnetic perturbation, the internal dynamic RMP coils were used for this experiment. The internal dynamic RMP coils can produce a 2.6 Gs kA^{-1} 2/1 mode which is much stronger than that achieved with the external static RMP coils. The internal RMP coils were powered from 0.407 s. The runaway current plateau did not decay compared to the unperturbed runaway plateau, although the RMP current was ramped up to 3 kA, which is about 7.8 Gs. There was no obvious decay of the runaway current during the application of RMP to several similar targets. The application of RMP corresponds to a $\delta B/B_T = 3.4 \times 10^{-4}$ magnetic perturbation, which has been shown to be effective to reduce runaway generation during disruptions. This indicates that the runaway current damping rate is insensitive to the magnetic perturbation as indicated by simulations and experiments [40, 41]. The runaway energy at the runaway plateau phase is about $W_r = 10.5$ MeV, estimated from the calculation in figure 14. Due to curvature drift, the drift orbits of the REs are shifted with respect to the magnetic surfaces [40]. The drift orbits increase with increasing runaway energy. The energetic REs with a large drift orbit become less sensitive to external magnetic perturbation. The simulation demonstrated that the loss of the energetic runaway beam is dominated by the shrinkage of the confinement region with increasing runaway energy, and is independent of the external magnetic perturbation [40, 41]. The confinement region shrinks due to the increase of runaway energy. The runaway beam inside the confinement region is not sensitive to the RMP. The effect of RMP on runaway loss decreased as the runaway energy increase. Thus the application of RMP is not practical for the suppression of a mature runaway beam during the runaway plateau phase in which the runaway beam has energy of the order of 10 MeV.

5. Summary

In summary, the regime of runaway current generation in MGI fast shutdown experiments has been investigated. It was found that pure He, pure Ne, and a mixture of He and Ar (9:1) are prone to induce runaway free fast shutdown as demonstrated in other devices [3, 9]. Moderate amount argon injection could generate a significant runaway current plateau. The regime of runaway generation by argon injection is about 7–70 times the plasma inventory. The amplitude of the runaway current decreases with increasing argon injection. The conversion ratio of the predisruption plasma current into runaway current in most argon induced disruptions is in the range of 30%–60%.

The threshold $B_T = 2$ T for runaway generation during disruptions is not general. It is found that the runaway current can be generated in J-TEXT with a much lower magnetic field of $B_T = 1.6$ T. The key parameter affecting runaway generation is the edge safety factor q_a instead of B_T in J-TEXT. The threshold of q_a decreases with increasing B_T.

The propagation of the cold front induced by the MGI gas jet in the plasma interior was observed using a fast frame camera. The cold front penetrated helically along the field lines preferentially toward the high field side, which is consistent with the simulation [31]. The cold front was stopped at a location near the $q = 2$ surface before the disruption. The soft x-ray imaging of the runaway beam during runaway current plateau phase provides information on the generation and confinement of REs. The maximum energy of the REs decreases with increasing runaway current. The runaway energy will reach its maximum value when the runaway current is close to zero. The maximum energy of REs in a 180 kA disruption plasma is about 21 MeV. The total energy of the runaway beam will reach a maximum kinetic energy when the runaway current is 50% of the predisruption plasma current.

RMP with an $m/n = 2/1$ mode was successfully applied to reduce runaway production during disruptions in J-TEXT. It was found that both the amplitude and the duration of the runaway current can be reduced by the application of RMP before the disruption as demonstrated in TEXTOR [26]. The success of runaway suppression using RMP for J-TEXT is

possible due to its small size and the short distance between the RMP coils and the plasma. RMP may not work for runaway suppression in large devices as indicated by the experimental results for JET. The simulations also indicate that RMP may not effective to achieve runaway suppression in ITER [41].

The application of RMP during the runaway current plateau phase demonstrated that the RMP is not effective in decoupling the energetic runaway beam even in the small device J-TEXT. When the runaway current builds up, the REs will reach a high energy which is less sensitive to external magnetic perturbation. The simulation demonstrated that the loss of the energetic runaway beam is dominated by the shrinkage of the confinement region, not the external magnetic perturbation [41]. The runaway beam inside the confinement region is not sensitive to the RMP. Thus the application of RMP is not practical for the suppression of a mature runaway beam during the runaway plateau phase in which the runaway beam has energy of the order of 10 MeV. This has important implications for the decoupling of runaway beams using external applied magnetic perturbation during the runaway current phase for the next generation ITER device.

Acknowledgments

This work was partially supported by the National Natural Science Foundation (Nos. 11275079, 11575068) and National Magnetic Confinement Fusion Science Program (Nos. 2015GB111002, 2013GB113003, 2015GB104004).

References

[1] Riccardo V. and JET EFDA Contributors 2003 *Plasma Phys. Control. Fusion* **45** A269
[2] Sebiiller F.C. 1995 *Plasma Phys. Control. Fusion* **37** A135
[3] Hender T.C. *et al* 2007 *Nucl. Fusion* **47** S128 (beginning of chapter)
[4] Pautasso G. *et al* 2007 *Nucl. Fusion* **47** 900
[5] Putvinski S. *et al* 1997 *Plasma Phys. Control. Fusion* **39** B157
[6] Commaux N. *et al* 2010 *Nucl. Fusion* **50** 112001
[7] Jaspers R. *et al* 1993 *Nucl. Fusion* **33** 1775
[8] Smith H.M. and Verwichte E. 2008 *Phys. Plasmas* **15** 072502
[9] Bozhenkov S.A. *et al* 2008 *Plasma Phys. Control. Fusion* **50** 105007
[10] Russo A.J. and Campbell R.B. 1993 *Nucl. Fusion* **33** 1305
[11] Gill R.D. *et al* 2000 *Nucl. Fusion* **40** 163
[12] Jaspers R. *et al* 1996 *Nucl. Fusion* **36** 367
[13] Plyusnin V.V. *et al* and JET EFDA Contributors 2006 *Nucl. Fusion* **46** 277
[14] Gál K. *et al* 2008 *Plasma Phys. Control. Fusion* **50** 055006
[15] Pautasso G. *et al* 1996 *Nucl. Fusion* **36** 1291
[16] Yoshino R. *et al* 1997 *Plasma Phys. Control. Fusion* **39** 313
[17] Taylor P.L. *et al* 1999 *Phys. Plasmas* **6** 1872
[18] Zeng L. *et al* 2013 *Phys. Rev. Lett.* **110** 235003
[19] Wongrach K. *et al* 2014 *Nucl. Fusion* **54** 043011
[20] Wongrach K. *et al* 2015 *Nucl. Fusion* **55** 053008
[21] Abdulaev S.S. *et al* 2015 *Phys. Plasmas* **22** 040704
[22] Granetz R.S. *et al* 2014 *Phys. Plasmas* **21** 072506
[23] Zhuang G. *et al* 2013 *Nucl. Fusion* **53** 104014
[24] Luo Y.H. *et al* 2014 *Rev. Sci. Instrum.* **85** 083504
[25] Yoshino R. *et al* 1999 *Nucl. Fusion* **39** 151
[26] Lehnen M. *et al* 2009 *J. Nucl. Mater.* **390–1** 740
[27] Zeng L. *et al* 2015 *J. Plasma Phys.* **81** 475810402
[28] Chen Z.Y. *et al* 2013 *Plasma Phys. Control. Fusion* **55** 035007
[29] Reux C. *et al* 2015 *Nucl. Fusion* **55** 093013
[30] Reux C. *et al* 2010 *Nucl. Fusion* **50** 095006
[31] Izzo V.A. *et al* 2015 *Nucl. Fusion* **55** 073032
[32] Chen Z.Y. *et al* 2012 *Rev. Sci. Instrum.* **83** 056108
[33] Martin-Solis J.R. *et al* 2006 *Phys. Rev. Lett.* **97** 165002
[34] Martin-Solis J.R. *et al* 2014 *Nucl. Fusion* **54** 083027
[35] Yoshino R. and Tokuda S. 2000 *Nucl. Fusion* **40** 1293
[36] Finken K. *et al* 2007 *Nucl. Fusion* **47** 91
[37] Finken K. *et al* 2006 *Nucl. Fusion* **46** S139
[38] Lehnen M. *et al* 2008 *Phys. Rev. Lett.* **100** 255003
[39] Riccardo V. *et al* 2010 *Plasma Phys. Control. Fusion* **52** 124018
[40] Papp G. *et al* 2011 *Nucl. Fusion* **51** 043004
[41] Papp G. 2011 *Plasma Phys. Control. Fusion* **53** 095004
[42] Papp G. *et al* 2012 *Plasma Phys. Control. Fusion* **54** 125008
[43] Matsuyama A. *et al* 2014 *Nucl. Fusion* **54** 123007